Rate Enhancements in Structural Transformations of Pt–Co and Pt– Ni Bimetallic Cathode Catalysts in Polymer Electrolyte Fuel Cells Studied by in Situ Time-Resolved X-ray Absorption...

ARTICLE *in* THE JOURNAL OF PHYSICAL CHEMISTRY C · JULY 2014

Impact Factor: 4.77 · DOI: 10.1021/jp504738p

8 AUTHORS, INCLUDING:

Nozomu Ishiguro
RIKEN
20 PUBLICATIONS **178** CITATIONS
SEE PROFILE

Sutasinee Kityakarn
Kasetsart University
10 PUBLICATIONS **53** CITATIONS
SEE PROFILE

Takashi Sasabe
Tokyo Institute of Technology
23 PUBLICATIONS **246** CITATIONS
SEE PROFILE

Kensaku Nagasawa
28 PUBLICATIONS **156** CITATIONS
SEE PROFILE

THE JOURNAL OF PHYSICAL CHEMISTRY C

Article

pubs.acs.org/JPCC

Rate Enhancements in Structural Transformations of Pt–Co and Pt–Ni Bimetallic Cathode Catalysts in Polymer Electrolyte Fuel Cells Studied by in Situ Time-Resolved X-ray Absorption Fine Structure

Nozomu Ishiguro,[†,‡] Sutasinee Kityakarn,[†,‡,§] Oki Sekizawa,[⊥] Tomoya Uruga,[⊥,∥] Takashi Sasabe,[†] Kensaku Nagasawa,[⊥] Toshihiko Yokoyama,[‡] and Mizuki Tada*[,†,‡]

[†]Research Center for Materials Science, Nagoya University, Furo, Chikusa, Nagoya, Aichi 464-8602, Japan

[‡]Institute for Molecular Science, 38 Nishigo-naka, Myodaiji, Okazaki, Aichi 444-8585, Japan

[§]Department of Chemistry, Faculty of Science, Kasetsart University, Bangkok 10903, Thailand

[⊥]Innovation Research Center for Fuel Cells, University of Electro-Communications, 1-5-1 Chofu, Tokyo 182-8585, Japan

[∥]Japan Synchrotron Radiation Research Institute, SPring-8, 1-1-1 Koto, Sayo, Hyogo 679-5198, Japan

Supporting Information

ABSTRACT: In situ time-resolved X-ray absorption fine structure spectra of Pt/C, Pt_3Co/C, and Pt_3Ni/C cathode electrocatalysts in membrane electrode assemblies (catalyst loading: 0.5 mg_{metal} cm^{-2}) were successfully measured every 100 ms for a voltage cycling process between 0.4 and 1.0 V. Systematic analysis of in situ time-resolved X-ray absorption near-edge structure and extended X-ray absorption fine structure spectra in the molecular scale revealed the structural kinetics of the Pt and Pt_3M (M = Co, Ni) bimetallic cathode catalysts under polymer electrolyte fuel cell operating conditions, and the rate constants of Pt charging, Pt–O bond formation/breaking, and Pt–Pt bond breaking/re-formation relevant to the fuel cell performances were successfully determined. The addition of the 3d transition metals to Pt reduced the Pt oxidation state and significantly enhanced the reaction rates of Pt discharging, Pt–O bond breaking, and Pt–Pt bond re-forming in the reductive process from 1.0 to 0.4 V.

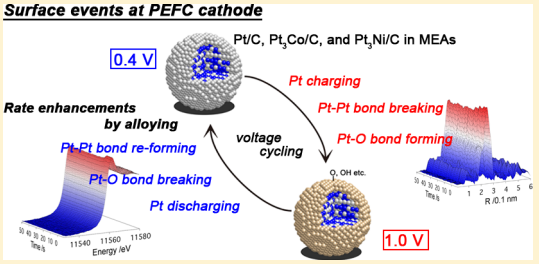

INTRODUCTION

Polymer electrolyte fuel cells (PEFCs) are among the most efficient clean energy technologies, and their practical application to automobiles has been widely developed. Nevertheless, their widespread adoption is obstructed by the high cost of precious metal electrocatalysts and their low durability under PEFC operating conditions.[1,2] At a cathode side, Pt-based electrocatalysts activate oxygen reduction reaction (ORR), where oxygen molecules are converted to water. However, strongly acidic conditions in the presence of Nafion in a membrane electrode assembly (MEA) often cause serious damage to the electrocatalysts particularly at the cathode under PEFC operating conditions.

Platinum-based bimetallic nanoparticles with 3d transition metals have been studied as one of the most promising candidates for cathode electrocatalysts for PEFCs to achieve the improvements of cell performances and durability.[3−12] Pt–Co alloy is representative of the Pt-based bimetallic catalysts with 3d transition metals. The fabrication of nanostructure with a Pt-alloy core and a thin Pt-rich shell, called Pt skin,[11−15] or sandwich segregation,[11,12,16,17] by acid treatment, potential cycling, or thermal annealing reported to show higher activity per Pt amount and more durable performances than Pt/C catalysts.

The effects and origin of alloying of Pt with 3d transition metals have been studied by various techniques such as theoretical calculations,[18−23] transmission electron microscopy,[11,12,24−28] and photoelectron spectroscopy.[7,29−32] The surface of Pt-based bimetallic catalysts can weaken the binding of oxygenated species to cathode catalysts, and the intrinsic ORR activity is enhanced by alloying.[11−23] Although such studies have revealed relationships between the enhancements in the ORR enhancements and the structures of the Pt-based bimetallic electrocatalysts, the details of dynamic surface events taking place at the cathode catalyst surface remain unclear, including individual redox processes under PEFC working conditions.

X-ray absorption fine structure (XAFS) spectroscopy is a powerful tool for investigating local structures of supported metal catalysts, which cannot be analyzed by X-ray diffraction.[33−35] The edges of transition of precious metals are in the hard X-ray region, and the high penetration power of hard X-rays allows us to obtain in situ XAFS spectra in the presence of water and fuel under PEFC working conditions.

Received: May 14, 2014
Revised: June 25, 2014
Published: July 4, 2014

Previously, the shrinks of Pt−M bond distances and the decreases of Pt d-band vacancies in Pt-based bimetallic catalysts, suggesting the shifts of Pt d-band center, have been investigated by XAFS analysis of the Pt-based bimetallic catalysts.[36−42] We have reported several papers on in situ time-resolved XAFS for Pt/C and Pt_3Co/C cathode catalysts under various PEFC operating conditions and discussed their structural kinetics for voltage cycling processes.[43−45] Because of limitations imposed by the X-ray flux at that time, the cathode catalyst loading of the MEA was restricted to 12 times higher than the practical one, but systematic analysis of the in situ time-resolved X-ray absorption near-edge structure (XANES) and extended X-ray absorption fine structure (EXAFS) spectra indicated differences in the reaction mechanism of Pt/C and Pt_3Co/C catalysts at cathode in the MEAs with thick cathode catalyst layers.[43]

In this paper, we report the results of in situ time-resolved XAFS analysis of Pt/C, Pt_3Co/C, and Pt_3Ni/C catalysts with practical catalyst loading (0.5 mg_{metal} cm^{-2}) in MEAs for a voltage cycling process between 0.4 and 1.0 V. Systematic analysis of the time-resolved XANES and EXAFS spectra revealed the structural kinetics of the Pt and Pt-based bimetallic catalysts for the voltage cycling process. We estimated all rate constants of the structural changes in the Pt and Pt-based bimetallic catalysts under identical conditions, and the differences observed suggested that alloying of Pt and 3d transition metals affects the structural kinetics of each redox process.

EXPERIMENTAL METHODS

PEFC. Pt/C (45.9 wt %; TEC10E50E, Tanaka Kikinzoku Kogyo (TKK) Co., Ltd., Japan), Pt_3Co/C (Pt 46.7 wt %, Co 5.4 wt % (Pt/Co = 2.6); TEC36E52, TKK) and Pt_3Ni/C (Pt 45.8 wt %, Ni 5.3 wt % (Pt/Ni = 2.6); TECNiE52, TKK) were used as cathode catalysts. Pd/C (47.7 wt %; TECPd(ONLY)-E50, TKK) was used as an anode catalyst. An MEA containing a Nafion NR-212 membrane (Sigma-Aldrich) was prepared by MicLab Co., Ltd., Japan. The size of the MEA was 3.0 × 3.0 cm^2, and catalyst loadings at the cathode and anode were 0.5 $mg_{PtM/Pd}$ cm^{-2} (M = none, Co, or Ni).

The MEA was evaluated by using a 13-layer single cell for in situ XAFS measurements based on the Japan Automobile Research Institute (JARI) standard cell.[46] The details of the cell are provided in our previous reports.[44] MEA was sandwiched into the XAFS cell with Teflon gaskets at both the cathode (thickness 200 μm) and the anode (180 μm) sides, after which they were affixed with 12 bolts (4 N m of torque was applied to tighten each bolt). Flows of pure H_2 (>99.99999% grade) to the anode and pure N_2 (>99.99995%; cyclic voltammogram (CV) and XAFS measurements) or pure air (G1 grade; aging, *IV* and XAFS measurements) to the cathode were regulated using mass-flow controllers. The gases were bubbled through humidifiers at 351 K using a commercial gas supply kit (CNF52742, NF Corporation). The humidified gases were supplied to the in situ XAFS cell at 353 K. The gas pressures and flow rates were 101.3 kPa and 150 mL min^{-1} at the anode (H_2) and 101.3 kPa and 600 mL min^{-1} at the cathode (N_2/air). The back-pressures were 2 kPa at the anode and about 3 kPa at the cathode. The cell voltage between the anode and the cathode was controlled using a P/G stat (VSP, BioLogic Science Instruments Co., Ltd.) with a current amplifier (VMP 3B-20, BioLogic Science Instruments).

All MEAs were subjected to aging before the in situ XAFS measurements. Dry air was fed to the cathode, and current was repeatedly applied 150 times in 19 fixed steps (0 A−0.01 A−0.04 A−0.12 A−0.16 A−0.22 A−0.27 A−0.33 A−0.48 A−0.66 A−1.31 A−1.95 A−2.60 A−3.25 A −3.82 A−4.56 A−5.20 A−5.85 A−6.50 A; 6 s per step). Cyclic voltammograms were recorded with H_2 flow (anode) and N_2 flow (cathode) before and after the in situ time-resolved XAFS measurements. Voltage was scanned between 0.05 and 1.0 V in 50 mV s^{-1} for 5 cycles, and the cell current was recorded every 10 ms. The electrochemically accessible surface area (ECSA) of the cathode catalysts after in situ XAFS measurements was estimated by the average charge density of hydrogen adsorption and desorption on a Pt surface (210 $\mu C\ cm_{Pt}^{-2}$). *IV* curves were obtained with H_2 flow (anode) and air flow (cathode) after the in situ time-resolved XAFS measurements in cathode N_2 flow and before the in situ time-resolved XAFS measurements in cathode air flow. Current was applied for 10 s at each step, and the cell voltage was recorded every 100 ms until the cell voltage became lower than 0.01 V. Average of the cell voltage for last 6 s in each current step was used for the plot of *IV* and power density curve.

TEM and STEM Analysis. TEM images of Pt/C, Pt_3Co/C, and Pt_3Ni/C catalysts in as-prepared and used MEAs were acquired with a field emission transmission electron microscope (FE-TEM) (JEM-3200, JEOL Co., Ltd.; accelerating voltage: 300 kV), and their images were used to analyze their particle size distribution. Scanning transmission electron microscopy/energy dispersive X-ray spectroscopy (STEM-EDS) analysis was performed on JEM-ARM200F (JEOL Co., Ltd.; accelerating voltage: 200 kV). Pt Mα, Co Kα, and Ni Kα X-ray fluorescence was used for the estimation of the atomic percentages of Co or Ni in Pt_3Co and Pt_3Ni particles.

In Situ XAFS and in Situ Time-Resolved XAFS. In situ Co/Ni K-edge quick-scanning XAFS (QXAFS) and Pt L_{III}-edge time-resolved QXAFS measurements were carried out at the BL36XU beamline at SPring-8 (8.0 GeV, 100 mA; Hyogo, Japan).[47] X-rays emitted from an in-vacuum tapered undulator were monochromatized by a Si(111) channel-cut compact monochromator. Higher harmonics have been rejected by two vertical mirrors settled between the monochromator and an I_0 ion chamber. Co/Ni K-edge XAFS spectra were recorded in fluorescence mode, and Pt L_{III}-edge XAFS spectra were recorded in transmission mode. Incident (I_0) and transmitted (I_1 and I_2) X-rays were detected by ion chambers filled with N_2 and N_2/Ar (85/15), respectively. Fluorescent X-rays (I_f) were detected by a 21-pixel germanium detector (Canberra EGPX 40×40×7-21PIX). The in situ XAFS cell with an MEA after the aging treatment was placed between the I_0 and I_1 ion chambers at a 45° angle to the optical axis to detect both transmitted and fluorescent X-rays detected by the germanium detector placed next to the cell at a 90° angle to the optical axis. Co, Ni, or Pt foil was set between the I_1 and I_2 ion chambers to calibrate the X-ray energy.

For the in situ Co/Ni K-edge QXAFS measurements, the voltage of the cell with the MEA after the aging treatment was set to 0.4 or 1.0 V by the P/G stat. After 1 min at each voltage, the Co K-edge (Pt_3Co/C) and Ni K-edge (Pt_3Ni/C) QXAFS spectra were recorded (15 min/spectrum × 3 scans at the Co K-edge and 13 min/spectrum × 2 scans at the Ni K-edge) at each voltage in either N_2 or air atmosphere at the cathode.

For in situ Pt L_{III}-edge time-resolved QXAFS measurements, the P/G stat was synchronized with a PC controlling the

dx.doi.org/10.1021/jp504738p | J. Phys. Chem. C 2014, 118, 15874−15883

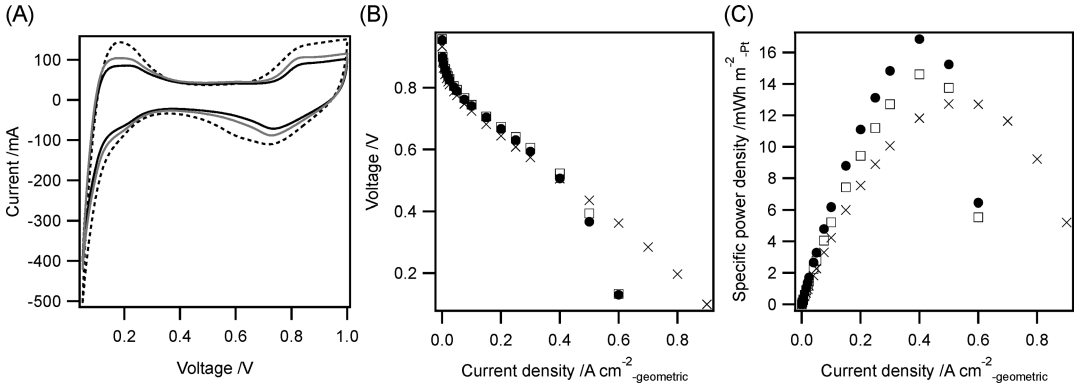

Figure 1. (A) Cyclic voltammograms (CVs) after XAFS measurements for Pt/C (dashed line), Pt_3Co/C (black solid line), and Pt_3Ni/C (gray solid line). Voltage scan range and scan rate of CV were 0.05−1.0 V and 50 mV s^{-1}, respectively. CVs were recorded at 353 K, in H_2 flow (101.3 kPa and 150 mL min^{-1}) at the anode, and in air flow (101.3 kPa and 600 mL min^{-1}) at the cathode with bubbling through humidifiers at 351 K. (B) *IV* curves and (C) specific power density curves: (×) Pt/C, (●) Pt_3Co/C, and (□) Pt_3Ni/C. Current in *IV* curves were applied for 10 s at each step. *IV* curves were recorded at 353 K, in H_2 flow (101.3 kPa and 150 mL min^{-1}) at the anode, and in N_2 flow (101.3 kPa and 600 mL min^{-1}) at the cathode with bubbling through humidifiers at 351 K. Specific power densities were calculated from cell power normalized by ECSA after the XAFS measurements.

QXAFS system by a gate signal (0 V → 5 V). The cell voltage protocol consisted of three voltage steps: 0.4 V (1.5 min) → 1.0 V (20 min) → 0.4 V (20 min), as shown in Figure S1. Within 10 s from either voltage change (0.4 V → 1.0 or 1.0 V → 0.4 V), a gate signal was sent from the P/G stat to start continuous QXAFS measurements. First, a series of QXAFS spectra were recorded every 100 ms (600 spectra over 60 s), after which 12 series were recorded every 100 ms (300 spectra over 30 s) with a block interval of 90 s. The measurements were first conducted in N_2 atmosphere and subsequently in air at the cathode.

Analysis of Co/Ni K-Edge and Pt L_{III}-Edge XAFS. The collected XANES and EXAFS spectra were analyzed either in Ifeffit (Athena and Artemis)[48] or in a custom program in Igor Pro 6.3, whose details were reported in our previous paper.[43−45] Phase shifts and the backscattering amplitude for each shell were calculated with the FEFF8.4 code[49,50] using structural parameters obtained from the crystal structures of Pt, PtO_2, PtCo, and PtNi.[51−54]

Two data of the observed time-resolved XAFS spectra were merged (100 ms × 2) for further analysis. A series of time-resolved XANES spectra were fitted by the following equation to estimate the edge energies and white line heights of the Pt L_{III}-edge.

$$\mu t(E) = \frac{a_1}{\pi}\left[\frac{\pi}{2} + \arctan\left(\frac{E - a_2}{a_3}\right)\right] + \frac{b_1}{1 + \left(\frac{E - b_2}{b_3}\right)^2}$$

The parameter of the Lorentz function (b_1) was used to estimate the white line height.

The merged Pt L_{III}-edge XAFS spectra obtained from 300 raw spectra in the 13th measurement block at each voltage step (0.4 V → 1.0 and 1.0 V → 0.4 V in either N_2 or air at the cathode) were initially analyzed to optimize the structural parameters for curve fitting analysis of time-resolved EXAFS Fourier transforms. Then the merged EXAFS Fourier transforms were analyzed by the curve fitting method. Some parameters (interatomic distance (R), correction-of-edge energy (ΔE_0), and Debye−Waller factor (σ^2) of the Pt−O shell and σ^2 of the Pt−Pt and Pt−M shells) were fixed at their optimized values estimated by the analysis of 300 merged spectra, as mentioned above.

The error ranges of the curve fitting analysis for the time-resolved QXANES spectra were estimated as 95% confidence intervals. The error ranges for the time-resolved EXAFS Fourier transforms in the curve fitting analysis were based on the definition in the Ifeffit code. Seven parameters (PEFC current/charge variation, recorded on the P/G stat; white line height of the Pt L_{III}-edge XANES; coordination number (CN) of Pt−Pt; CN of Pt−M; CN of Pt−O; R of Pt−Pt; and R of Pt−M) were plotted against time (t).

The rate constants of these parameters were estimated by curve fitting using an exponential function or linear combinations of exponential and linear functions, taking into account the error weighting given by the inverse of the error. For the curve fitting, the initial value of each plot was independently calculated as the average of each parameter for the 10 s period at each step before the voltage was changed. Curve fitting with exponential functions was performed for the period of 0−50 s after the voltage was changed.

RESULTS AND DISCUSSION

Electrochemical Analysis and Properties of Pt/C, Pt_3Co/C, and Pt_3Ni/C Cathode Catalysts in MEAs. The particle sizes of the Pt and Pt-based bimetallic catalysts in the fresh MEAs were examined by TEM (Figure S2). The average sizes of Pt, Pt_3Co, and Pt_3Ni particles in the MEAs were estimated to be 2.6 ± 0.7, 4.9 ± 1.7, and 4.2 ± 1.4 nm, respectively (Table S1).

Figure 1 shows the CVs, *IV* curves, and the specific power density curves of the MEAs with the Pt/C, Pt_3Co/C, and Pt_3Ni/C cathode catalysts. ECSAs of the Pt/C, Pt_3Co/C, and Pt_3Ni/C in the MEAs, which were estimated from H_2 desorption/adsorption charge in the CVs, were 57 $m_{Pt}^2\ g_{Pt}^{-1}$, 40 $m_{Pt}^2\ g_{PtCo}^{-1}$, and 48 $m_{Pt}^2\ g_{PtNi}^{-1}$, respectively (Table S1). Although the ECSAs of the Pt catalysts decreased by 5−10% after the in situ time-resolved XAFS measurements, the order of the ECSAs (Pt/C > Pt_3Ni/C > Pt_3Co/C) did not change during the experiments. Current increase from 0.6 V in the forward scan on Pt/C (Figure 1A) was assigned to the formation of $Pt-OH_{ads}$, and that above 0.8 V was the formation of $Pt-O_{ads}$.[31] Negative current peak in the reverse scan was observed on Pt/C between 1.0 and 0.4 V, and the positive shifts of the peaks on Pt_3Co/C and Pt_3Ni/C were observed,

dx.doi.org/10.1021/jp504738p | J. Phys. Chem. C 2014, 118, 15874−15883

indicating more reductive behaviors of Pt_3Co/C and Pt_3Ni/C than Pt/C.

The specific power densities related to the activity of surface Pt catalysts were also estimated. The maximum power densities of Pt/C, Pt_3Co/C, and Pt_3Ni/C in the specific power density curves (Figure 1C) were 13 mWh m_{Pt}^{-2}, 17 mWh m_{Pt}^{-2}, and 15 mWh m_{Pt}^{-2}, respectively. The order of the specific power densities was Pt_3Co/C > Pt_3Ni/C > Pt/C.

In Situ Co/Ni K-Edge XAFS of Pt_3Co/C and Pt_3Ni/C. In situ Co/Ni K-edge XAFS spectra of the Pt_3Co/C and Pt_3Ni/C catalysts were recorded under PEFC operating conditions, and the local structure of Co/Ni species was investigated. Figure 2

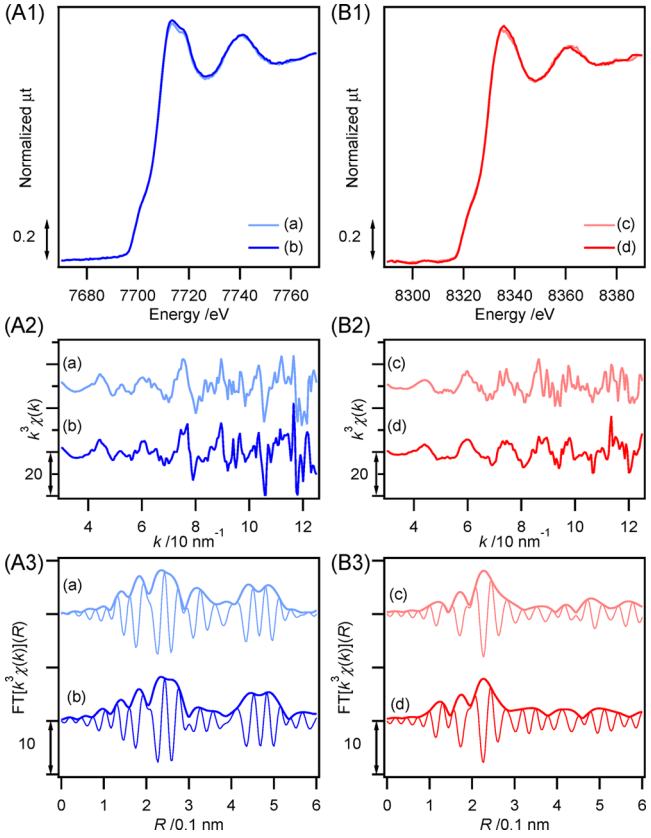

Figure 2. In situ Co K-edge and Ni K-edge XAFS of (A) Pt_3Co/C and (B) Pt_3Ni/C cathode catalysts in the MEAs. (A1) Co K-edge XANES spectra, (A2) Co K-edge k^3-weighted EXAFS oscillations, (A3) Co K-edge k^3-weighted EXAFS Fourier transforms at k = 30−120 nm^{-1}, (B1) Ni K-edge XANES spectra, (B2) Ni K-edge k^3-weighted EXAFS oscillations, (B3) Ni K-edge k^3-weighted EXAFS Fourier transforms at k = 30−120 nm^{-1}. (a) Pt_3Co/C at 0.4 V in N_2, (b) Pt_3Co/C at 1.0 V in N_2, (c) Pt_3Ni/C at 0.4 V in N_2, and (d) Pt_3Ni/C at 1.0 V in N_2.

shows Co and Ni K-edge XANES spectra and their k^3-weighted EXAFS oscillations of Pt_3Co/C and Pt_3Ni/C at 0.4 and 1.0 V in N_2 atmosphere at the cathode. The differences in the shapes Co K-edge XANES for Pt_3Co/C or those of Ni K-edge XANES for Pt_3Ni/C were negligible at the investigated cell voltages (Figures 2A1 and 2B1). The loading of Co or Ni atoms were 0.052 mg cm^{-2} in the MEAs, and this low loading of these atoms prevented us from conducting curve fitting analysis of their EXAFS Fourier transforms (Figures 2A3 and 2B3), but their EXAFS oscillations (Figures 2A2 and 2B2) indicated negligible differences in local coordination around Co or Ni at the cell voltages. We have reported similar negligible responses at the Co site at 0.4 and 1.0 V in N_2 on an MEA with a similar Pt_3Co/C catalyst but different catalyst loading (6 mg_{PtCo} cm^{-2}) by Co K-edge XANES and EXAFS.[43] These results indicated that the electronic states and local structures of Co and Ni in the Pt_3Co/C and Pt_3Ni/C catalysts were inert to the voltage cycling process under identical conditions.

Pt L_{III}-Edge XAFS of Pt/C, Pt_3Co/C, and Pt_3Ni/C. Figure 3 and Figures S3−S5 show in situ Pt L_{III}-edge XANES, k^3-

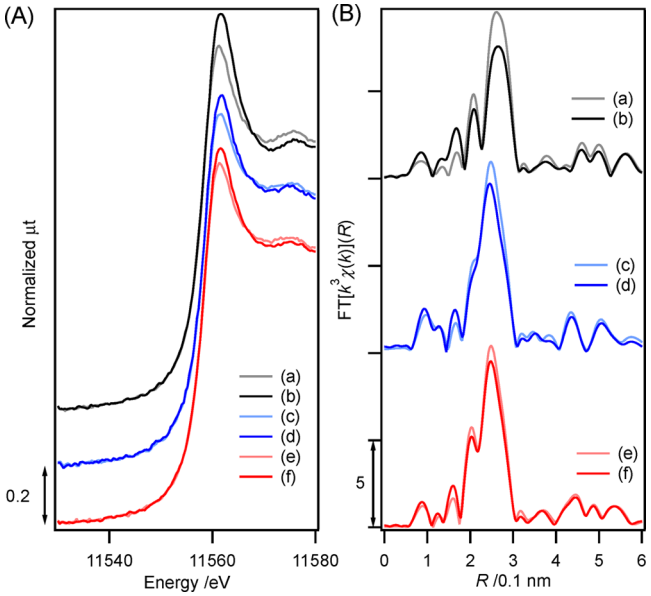

Figure 3. In situ Pt L_{III}-edge XAFS spectra of the Pt/C, of Pt_3Co/C, and Pt_3Ni/C cathode catalysts in the MEAs. (A) Pt L_{III}-edge XANES spectra, (B) k^3-weighted EXAFS Fourier transforms at k = 30−140 nm^{-1}. (a) Pt/C at 0.4 V in N_2, (b) Pt/C at 1.0 V in N_2, (c) Pt_3Co/C at 0.4 V in N_2, (d) Pt_3Co/C at 1.0 V in N_2, (e) Pt_3Ni/C at 0.4 V in N_2, and (f) Pt_3Ni/C at 1.0 V in N_2.

weighted EXAFS oscillations, and their Fourier transforms (300 merged spectra) for the Pt/C, Pt_3Co/C, and Pt_3Ni/C cathode catalysts in MEAs at the cell voltages of 0.4 and 1.0 V in N_2 at the cathode. Oxidation of Pt was observed at 1.0 V in N_2 for all three catalysts, as indicated by the increase in the Pt L_{III}-edge XANES white line heights (Figure 3A).

The structural parameters of the local coordination of the Pt/C, Pt_3Co/C, and Pt_3Ni/C catalysts in the MEAs were also examined by conducting curve fitting analysis of the Pt L_{III}-edge EXAFS Fourier transforms (Tables S2−S4). First, we performed curve fitting analysis of the EXAFS Fourier transforms of the Pt/C cathode catalyst at 0.4 and 1.0 V in N_2. At 0.4 V, the Pt catalyst was reduced and the Pt−O contribution was negligible; its Fourier transform was fitted with a single Pt−Pt shell at 0.275 ± 0.001 nm (Table S2a). At 1.0 V, its Fourier transform was fitted with two shells of Pt−O at 0.199 ± 0.003 nm and Pt−Pt at 0.275 ± 0.001 nm (Table S2b). We estimated the contribution of the Pt−O bond at 0.4 V in N_2; the CNs of Pt−Pt and Pt−O were estimated to be 8.7 ± 0.3 and 0.2 ± 0.1 (Table S2c), respectively. At 1.0 V in N_2, the CNs of Pt−Pt and Pt−O were 6.9 ± 0.3 and 0.9 ± 0.1, respectively (Table S2d), indicating that the surface of the Pt catalyst was oxidized at 1.0 V. To further analyze the series of time-resolved EXAFS Fourier transforms with a shorter acquisition time (100 ms ×2), R, ΔE_0, σ^2 of Pt−O, and σ^2 of

dx.doi.org/10.1021/jp504738p | J. Phys. Chem. C 2014, 118, 15874−15883

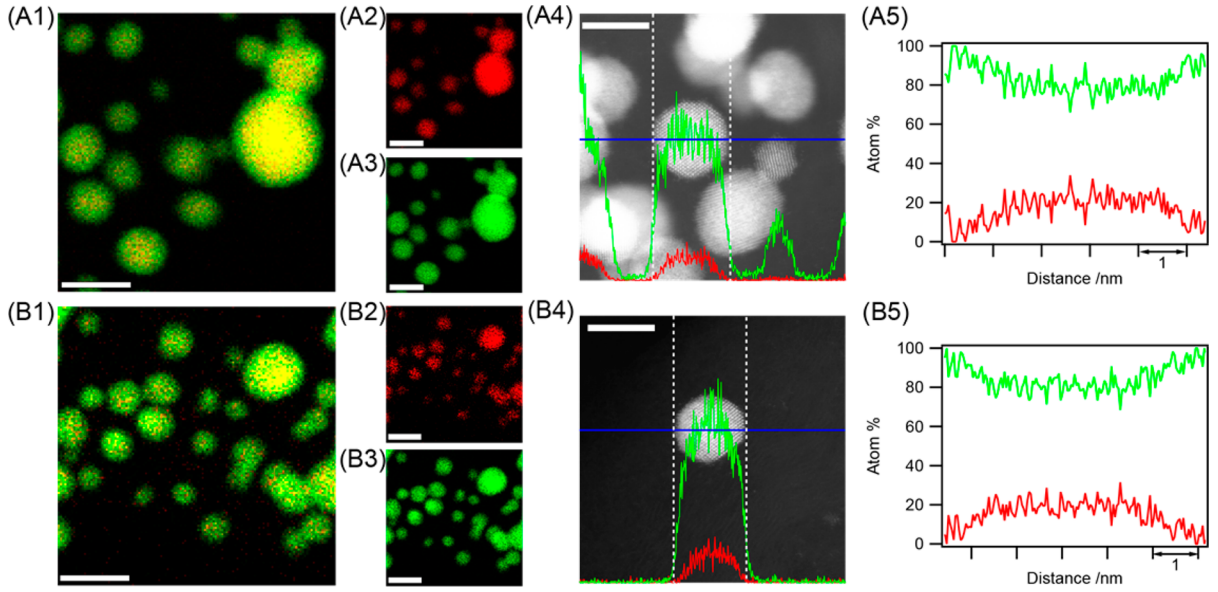

Figure 4. STEM-EDS mapping images and line profiles of (A) Pt_3Co and (B) Pt_3Ni nanoparticles in the MEAs after the in situ XAFS measurements. (1) EDS mapping images overwritten Co/Ni Kα and Pt Mα intensities, EDS mapping images of (2) Co/Ni Kα intensity and (3) Pt Mα intensity, (4) STEM images and EDS line profiles of Co/Ni Kα (red line) and Pt Mα (green line) on the blue lines, and (5) the line profiles of the atomic ratios of Pt (green line) and Co/Ni (red line) for the particle in (4) (on the blue lines). Scale bars in (1)−(3) are 10 nm and (4) 5 nm.

Pt−Pt were fixed at their optimized values according to the former two curve fitting results.

The EXAFS Fourier transforms of Pt_3Co/C were also analyzed in a similar manner as those of Pt/C. Thus, Pt_3Co/C at 0.4 V in N_2 was fitted with two shells of Pt−Pt at 0.272 ± 0.001 nm and Pt−Co at 0.265 ± 0.001 nm (Table S3a) and at 1.0 V in N_2 with three shells of Pt−Pt at 0.272 ± 0.001 nm, Pt−Co at 0.266 ± 0.003 nm, and Pt−O at 0.198 ± 0.006 nm (Table S3b). Then, the CNs of Pt−Pt, Pt−Co, and Pt−O at 0.4 V in N_2 were estimated to be 8.2 ± 0.4, 1.7 ± 0.2, and 0.1 ± 0.1, respectively (Table S3c), whereas those at 1.0 V in N_2 were 7.1 ± 0.4, 1.7 ± 0.2, and 0.4 ± 0.1, respectively (Table S3d). Based on the results of Pt L_{III}-edge and Co K-edge EXAFS analysis, Pt in the Pt−Co bimetallic particles was oxidized at 1.0 V despite the negligible structural changes at the Co side.

The EXAFS Fourier transforms of the Pt_3Ni/C catalyst showed similar trends to those of Pt_3Co/C. Thus, Pt_3Ni/C at 0.4 V in N_2 was fitted with two shells of Pt−Pt at 0.272 ± 0.001 nm and Pt−Ni at 0.263 ± 0.003 nm (Table S4a) and at 1.0 V in N_2 with three shells of Pt−Pt at 0.272 ± 0.001 nm, Pt−Ni at 0.264 ± 0.003 nm, and Pt−O at 0.198 nm, whose R, ΔE_0, and σ^2 were fixed at the optimized values obtained for Pt_3Co/C (Table S4b). The optimized σ^2 values of Pt−Pt and Pt−Ni were used for further curve fitting analysis of Pt_3Ni/C, and the CNs of Pt−Pt, Pt−Ni, and Pt−O at 0.4 V were estimated to be 7.9 ± 0.5, 2.0 ± 0.3, and 0.0 ± 0.1, respectively (Table S4c), whereas those at 1.0 V were 6.9 ± 0.5, 2.0 ± 0.3, and 0.3 ± 0.1, respectively (Table S4d).

We also measured the XAFS spectra of the Pt cathode catalysts in air at the cathode. At 1.0 V, all the cathode catalysts were oxidized similarly to those at 1.0 V in N_2 (Tables S2−S4 and Figures S3−S5). The CNs of Pt/C at 1.0 V in air were 6.8 ± 0.3 (Pt−Pt at 0.275 nm) and 0.8 ± 0.1 (Pt−O at 0.199 nm) (Table S2f); the CNs of Pt_3Co/C were 7.1 ± 0.6 (Pt−Pt at 0.272 nm), 1.7 ± 0.3 (Pt−Co at 0.265 nm), and 0.3 ± 0.1 (Pt−O at 0.198 nm) (Table S3f); the CNs of Pt_3Ni/C were 6.2 ± 0.5 (Pt−Pt at 0.272 nm), 2.0 ± 0.3 (Pt−Ni at 0.263 nm), and 0.3 ± 0.1 (Pt−O at 0.198 nm) (Table S4f). On the other hand, at 0.4 V in air, the Pt catalysts were only slightly oxidized compared to those at 0.4 V in N_2. The CNs of Pt/C were 7.2 ± 0.3 (Pt−Pt) and 0.7 ± 0.1 (Pt−O) (Table S2e); the CNs of Pt_3Co/C were 7.6 ± 0.6 (Pt−Pt), 1.6 ± 0.2 (Pt−Co), and 0.1 ± 0.1 (Pt−O) (Table S3e); the CNs of $Pt_3/Ni/C$ were 7.0 ± 0.8 (Pt−Pt), 1.9 ± 0.5 (Pt−Ni), and 0.1 ± 0.2 (Pt−O) (Table S4e). At 0.4 V in air, ORR is steady at the cathode, and the XAFS spectra reflected the local coordination of the Pt catalysts under steady-state ORR conditions. A similar trend was observed in our previous report on the Pt/C catalyst.[44,45]

Structures of Pt-Based Bimetallic Catalysts. Commercial Pt_3Co/C is reported to consist of Pt−Co bimetallic nanoparticles with a skeleton-type structure, and the following galvanostatic or annealing procedure leads to surface reconstruction to a Pt-rich skin surface with a Pt−Co bimetal core.[11−17] The STEM-EDS analysis of Pt_3Co nanoparticles in the MEA after the in situ XAFS measurements supports the reported structure (Figure 4A). Figure 4A1 represents overwritten images of Co Kα and Pt Mα EDS analysis on the catalyst particles. The core of the particles was colored in yellow, while their rim was in green, suggesting the Pt-rich skin surface on the sample. Negative correlation was observed between Pt atomic ratio of the Pt_3Co particles and their particle sizes, in agreement with EELS and STEM analysis by Xin et al.[24−26] Similar results were obtained on the Pt_3Ni catalyst (Figure 4B).

The bond distances for Pt−Pt and Pt−Co in Pt_3Co/C at 0.4 V in N_2, where the nanoparticles at the cathode seem to be reduced to metallic states, were estimated to be 0.272 and 0.265 nm, respectively, from the analysis of Pt L_{III}-edge EXAFS (Table S3). Both of these values are shorter than of the value for pure Pt (0.277 nm) but longer than that of pure Co (0.251 nm), as previously reported,[43] suggesting the formation of bimetallic structures. The bond distances in the Pt_3Ni/C catalyst were similar (the Pt−Pt and Pt−Ni bond distances at 0.4 V in N_2 were estimated to be 0.272 and 0.263 nm,

dx.doi.org/10.1021/jp504738p | J. Phys. Chem. C 2014, 118, 15874−15883

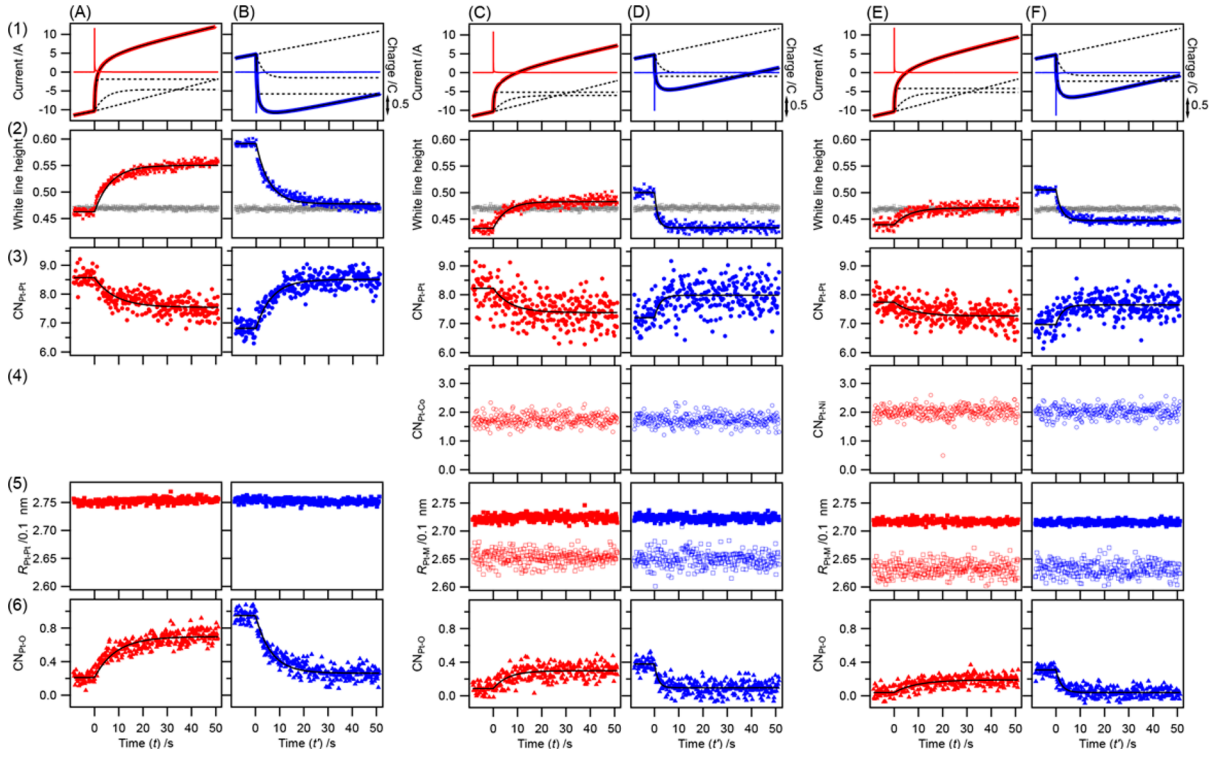

Figure 5. Time profiles of (1) electric current and charge, (2) Pt L_{III}-edge white line height, (3) CN of Pt−Pt bonds, (4) CN of Pt−M (Co, Ni) bonds, (5) *R* of Pt−M (Pt, Co, Ni) bonds, and (6) CN of Pt−O bonds for the voltage cycling process. (A) Pt/C, 0.4 V → 1.0 V in N_2, (B) Pt/C, 1.0 V → 0.4 V in N_2, (C) Pt_3Co/C, 0.4 V → 1.0 V in N_2, (D) Pt_3Co/C, 1.0 V → 0.4 V in N_2, (E) Pt_3Ni/C, 0.4 V → 1.0 V in N_2, and (F) Pt_3Ni/C, 1.0 V → 0.4 V in N_2. Red/blue solid lines: electric current in the cell; bold lines: electric charge in the cell; ×: white line height; ●, ■: Pt−Pt; ○, □: Pt−M (M: Co, Ni); and ▲: Pt−O. Black solid lines represent curve-fitted data, and black dashed lines in (1) represent each component in the curve fitting. Gray markers in (2) correspond to the white line height of Pt foil (reference).

respectively (Table S4), suggesting an bimetallic structure of Pt−Ni similar to that of Pt−Co.

We reported negative responses of the Co atoms of the Pt_3Co/C cathode catalyst in the MEA (6 mg_{PtCo} cm^{-2}) for voltage cycling process between 0.4 and 1.0 V.[43] In contrast, Pt L_{III}-edge XAFS responded positively to the voltage changes. The surface of the Pt−Co particles was rich in Pt, and Co atoms inside the core of the bimetallic particles did not form Co−O bonds at 1.0 V.[43] In the present MEAs with low catalyst loading, similar negligible changes in the Co and Ni K-edge XAFS spectra (Figure 2) indicated similar core−shell structures with Pt-rich shells and bimetallic cores for both the Pt_3Co and the Pt_3Ni catalysts.

In Situ Pt L_{III}-Edge Time-Resolved XAFS Analysis of Pt/C, Pt_3Co/C, and Pt_3Ni/C. The temporal variations in the structural parameters of Pt and Pt-based bimetallic cathode catalysts in the MEAs were investigated by time-resolved QXAFS analysis at the Pt L_{III}-edge for the voltage cycling process in N_2. A series of in situ time-resolved QXANES spectra and the Fourier transforms of k^3-weighted QEXAFS oscillations during the voltage cycling process (0.4 V → 1.0 V → 0.4 V) in N_2 were obtained for Pt/C, Pt_3Co/C, and Pt_3Ni/C (Figures S6−S8).

For the voltage change from 0.4 to 1.0 V, increases in the Pt L_{III}-edge white line height were observed in a series of QXANES spectra (Figures S6−S8 (A1)), and the reverse process from 1.0 to 0.4 V caused reversible decrease in the white line height (Figures S6−S8 (B1)). In the series of EXAFS Fourier transforms, the formation of Pt−O and the dissociation of Pt−Pt bonds were observed for the process from 0.4 to 1.0 V (Figures S6−S8 (A2)). Reversible bond dissociation of Pt−O and bond reformation of Pt−Pt were observed for the reverse process (Figures S6−S8 (B2)).

We analyzed electrochemical data and in situ time-resolved XAFS spectra for both voltage cycling processes, and the results are summarized in Figure 5. Current in the cell recorded on the P/G stat changed immediately after the voltage was changed (Figure 5 (1)). The actual electrochemical reactions in the cell due to the voltage change were estimated by subtracting the background current in the cell (dotted lines in Figure 5 (1)).

In Figure 5 (2), we plotted the changes in the white line heights of the in situ time-resolved QXANES spectra for the voltage cycling process in N_2. The white line height gradually increased after the voltage was changed from 0.4 to 1.0 V and dropped after the reverse voltage operation. It should be noted that there were significant differences in both variation range and absolute value between the white line heights of the Pt/C, Pt_3Co/C, and Pt_3Ni/C catalysts. In the case of Pt/C (Figures 5A2 and 5B2), the white line height at 0.4 V was similar to that of Pt foil, indicating that the valence state of the Pt/C catalyst was metallic at 0.4 V. In contrast, the Pt_3Co/C (Figures 5C2 and 5D2) and Pt_3Ni/C (Figures 5E2 and 5F2) catalysts at 0.4 V were more reduced, indicating electron-rich states under these conditions, which suggests that the alloying of Pt with Co and Ni caused a decrease in the energy level of the 5d-band center of the Pt-based bimetallic catalysts.[7] We have previously reported similar results for an MEA with the Pt_3Co/C catalyst (6 mg_{PtCo} cm^{-2}).[43]

Curve fitting analysis of the in situ time-resolved EXAFS Fourier transforms revealed the structural parameters of the

dx.doi.org/10.1021/jp504738p | J. Phys. Chem. C 2014, 118, 15874−15883

Table 1. Rate Constants of the Electrochemical Processes and Structural Changes in the Pt/C, Pt_3Co/C, and Pt_3Ni/C Cathode Catalysts in the MEAs for the Voltage Cycling Process between 0.4 and 1.0 V in N_2 Atmosphere at the Cathode

		rate constant/s^{-1}		
	parameter	Pt/C	Pt_3Co/C	Pt_3Ni/C
0.4 V → 1.0 V	electrochemical process (k_{e1})	2.84 ± 0.02	3.63 ± 0.03	3.56 ± 0.03
	electrochemical process (k_{e2})	0.226 ± 0.001	0.201 ± 0.001	0.207 ± 0.001
	white line height (k_{Pt})	0.150 ± 0.005	0.19 ± 0.01	0.16 ± 0.02
	CN_{Pt-Pt} (k_{Pt-Pt})	0.12 ± 0.01	0.14 ± 0.03	0.13 ± 0.05
	CN_{Pt-O} (k_{Pt-O})	0.113 ± 0.007	0.16 ± 0.03	0.11 ± 0.02
1.0 V → 0.4 V	electrochemical process (k'_{e1})	3.85 ± 0.02	6.82 ± 0.04	6.29 ± 0.04
	electrochemical process (k'_{e2})	0.378 ± 0.002	0.454 ± 0.001	0.445 ± 0.002
	white line height (k'_{Pt})	0.186 ± 0.006	0.75 ± 0.06	0.45 ± 0.02
	CN_{Pt-Pt} (k'_{Pt-Pt})	0.15 ± 0.01	0.4 ± 0.2	0.4 ± 0.1
	CN_{Pt-O}(k'_{Pt-O})	0.155 ± 0.007	0.7 ± 0.1	0.47 ± 0.06

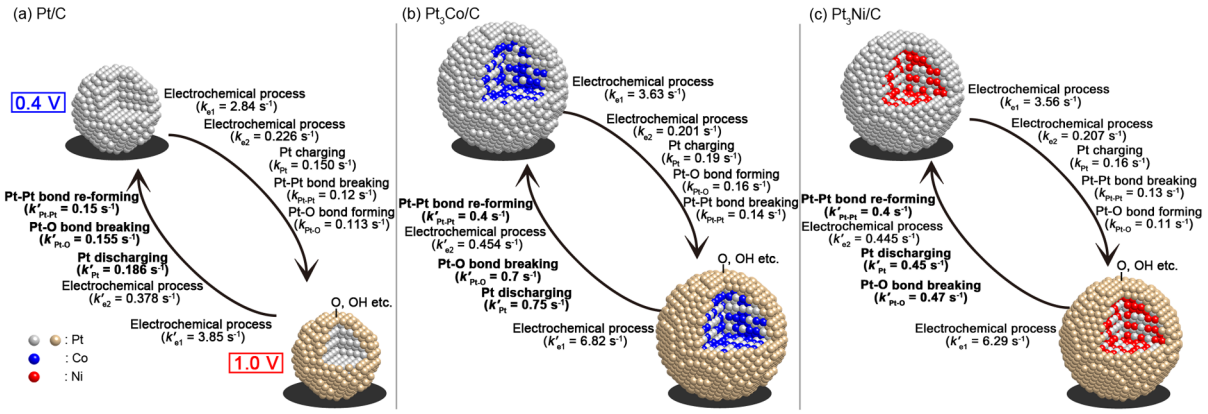

Figure 6. Structural kinetics of the surface events for the voltage-cycling processes between 0.4 and 1.0 V in N_2 atmosphere (cathode): (a) Pt/C, (b) Pt_3Co/C, and (c) Pt_3Ni/C.

three catalysts during the voltage cycling process. We found significant differences in CN between Pt−Pt and Pt−O bonds for all catalysts (Figure 5 (3) and (6)). For the voltage change from 0.4 to 1.0 V, partial dissociation of the Pt−Pt bonds was observed, accompanied by the formation of Pt−O bonds. Note that the changes in CNs of Pt−Co and Pt−Ni were negligible (Figure 5 (4)). These results agree with the structural model of Pt-based bimetallic catalysts (Pt-rich surface and Pt-M bimetallic core). The Pt−Pt and Pt−M (M: Co or Ni) bond distances remained constant during the voltage cycling process (Figure 5 (5)).

It was obvious that the variation ranges of these estimated parameters for Pt_3Co/C and Pt_3Ni/C between 0.4 and 1.0 V were much narrower than those for Pt/C (Figure 5). The variation ranges of the white line height (Δ_{Pt}) and CNs of Pt−Pt (Δ_{Pt-Pt}) and Pt−O(Δ_{Pt-O}) between 0.4 and 1.0 V for Pt/C were 0.128, 1.75, and 0.74, respectively; those for Pt_3Co/C were 0.067, 1.02, and 0.29; and those for Pt_3Ni/C were 0.065, 0.78, and 0.27. Although Pt/C, Pt_3Co/C, and Pt_3Ni/C have different particle sizes (2.6 ± 0.7, 4.9 ± 1.7, and 4.2 ± 1.4 nm, respectively) and active surface areas (57, 40, and, 48 m^2 g_{metal}^{-1}, respectively), the variation ranges of these parameters (Δ_{Pt}, Δ_{Pt-Pt}, and Δ_{Pt-O}) of Pt_3Co/C and Pt_3Ni/C were considerably smaller than those of Pt/C.

Finally, we fitted the plots of the current and charge in the cell, the white line heights of the Pt L_{III}-edge XANES spectra, and the CNs of Pt−Pt and Pt−O against time with exponential functions. The rate constants of these parameters were obtained as k from the fitted data in Figure 5.

Structural Kinetics and Rate Enhancements of Pt-Based Bimetallic Catalysts during the Voltage Cycling Process. The four electronic and structural parameters were fitted with linear combinations of exponential functions to estimate the rate constants k (Table 1 and Table S5). The charges in the fuel cell could not be fitted with a single-exponential function, and therefore they were fitted with a linear combination of two exponential functions. Their rate constants for the voltage change from 0.4 to 1.0 V were denoted as k_{e1} and k_{e2}, and those for the reverse process (1.0 to 0.4 V) were denoted as k'_{e2} and k'_{e2}.

In contrast, the other parameters were able to be fitted with a single-exponential function. The rate constants of the changes in the Pt L_{III}-edge white line height, representing changes in Pt oxidation state, were denoted as k_{Pt} and k'_{Pt}, and those in the CNs of Pt−Pt and Pt−O were denoted as k_{Pt-Pt}, k'_{Pt-Pt}, k_{Pt-O}, and k'_{Pt-O}. The CNs of Pt−Co and Pt−Ni were regarded as constant, and therefore the rate constants of these parameters were not estimated.

The rate constants of Pt/C, Pt_3Co/C, and Pt_3Ni/C for the voltage step of 0.4 V → 1.0 V in N_2 were ordered as shown in Figure 6. Electrochemical processes immediately proceeded and then structural changes of the Pt catalysts (charging, Pt−Pt bond breaking, and Pt−O bond formation) proceeded. The respective orders of the reaction processes were similar for the Pt/C, Pt_3Co/C, and Pt_3Ni/C catalysts. This indicated that the corresponding oxidation mechanisms were similar under identical conditions (Figure 6). It should be noted that the

dx.doi.org/10.1021/jp504738p | J. Phys. Chem. C 2014, 118, 15874−15883

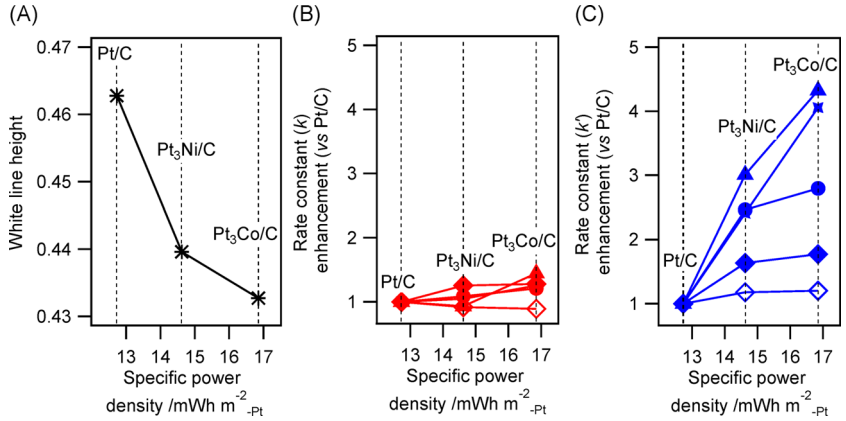

Figure 7. (A) Relationship between Pt L_{III}-edge XANES white line height of Pt and Pt-bimetallic cathode catalysts at 0.4 V in N_2 and specific power density. (B, C) Relationships between enhancements in the structural rate constants for the voltage cycling process in N_2 and specific power density. (B) 0.4 V → 1.0 V and (C) 1.0 V → 0.4 V. ♦: k_{e1} or k'_{e1}; ◊: k_{e2} or k'_{e2}; ×: k_{Pt} or k'_{Pt}, ●: k_{Pt-Pt} or k'_{Pt-Pt}; and ▲: k_{Pt-O} or k'_{Pt-O}.

rates of the structural transformation for the three cathode catalysts were in the order of Pt_3Co/C > Pt_3Ni/C > Pt/C.

For the reverse voltage change (1.0 V → 0.4 V) in N_2, all the reaction rates were faster than those in the reverse process of 0.4 V → 1.0 V on the three cathode catalysts. In Pt/C, two-electron processes took place first, followed by structural changes in the Pt catalyst (reduction, Pt−O bond breaking, and Pt−Pt bond re-formation). Pt_3Co/C and Pt_3Ni/C showed significant increases in the rate constants of the structural changes in the Pt-based bimetallic catalysts. The rates of structural transformation for the three cathode catalysts in this process were in the order of Pt_3Co/C > Pt_3Ni/C > Pt/C, where the increments compared to Pt/C were larger than those for the 0.4 V → 1.0 V process. The mechanisms of Pt reduction in the voltage process of 1.0 V → 0.4 V on the Pt/C, Pt_3Co/C, and Pt_3Ni/C catalysts were also considered to assemble each other as illustrated in Figure 6.

We also investigated the structural kinetics of the Pt and Pt-based bimetallic cathode catalysts for the voltage cycling process between 0.4 and 1.0 V in air, whose Pt L_{III}-edge time-resolved XAFS spectra and profiles are presented in Figures S9−S12 and Table S6. At 0.4 V in air, the structural parameters of the Pt catalysts were in the range between those at 0.4 V in N_2 and those at 1.0 V in N_2 (Figure S12). The parameters at 1.0 V in air were at similar levels to those at 1.0 V in N_2. The gaps in the structural parameters between 0.4 and 1.0 V in air were negligible, and therefore the rate constants of these structural changes in air are not discussed in detail in this paper.

Effects of Alloying on Structural Kinetics. The white line height levels at 0.4 V in N_2 (t < 0 s in Figure 5 (A2, C2, and E2)) reflect the unoccupied 5d-band densities of Pt in the metallic Pt/C, Pt_3Co/C, and Pt_3Ni/C catalysts, which are related to their Pt oxidation states. The average value of the white line height of Pt/C at 0.4 V in N_2 was estimated to be 0.4628 ± 0.0007, which was similar to that of Pt foil (0.4697 ± 0.0001), indicating that Pt/C at 0.4 V was reduced in the same way as Pt^0. In comparison, the average values for the Pt_3Co/C and Pt_3Ni/C catalysts were 0.433 ± 0.001 and 0.440 ± 0.001, respectively, which were smaller than that of Pt foil, represented the electron-rich states of the Pt-based bimetallic catalysts with the down shifts of their 5d-band centers reported by Stamenkovic et al.[13−15] They reported that the shift of the 5d-band center level for the skin or skeleton surfaces of catalyst alloys of Pt and 3d transition metals strongly affects the Pt−O bond energy, the adsorption energy of O_2 and other ORR intermediates, and the reactivity of Pt surfaces for ORR.

Figure 7 and Figure S13 show relationship between the PEFC performance and Pt L_{III}-edge XANES white line heights at 0.4 V in N_2 and those between the extent of rate enhancement in the structural kinetics for the voltage cycling process for Pt/C, Pt_3Co/C, and Pt_3Ni/C cathode catalysts. The specific power density of the cell has a downside correlation with the white line height (Figure 7A), which is in agreement with a report by Stamenkovic et al., which elucidated the linearity of ORR activity and d-band center shift between Pt_3Co, Pt_3Ni, and polycrystalline Pt.[13−15]

Although we did not investigate the influence of the particle sizes of the cathode catalysts to the structural kinetics, there are reports on the influence of Pt particle sizes to PEFC performances. Nesselberger et al. reported that the particle sizes of Pt catalysts (below 5 nm size) were negligible for ORR reaction kinetics,[55] and similar trends were reported by Perez-Alonso et al.[56] These results would be suggested that the rate enhancements on Pt_3Co/C and Pt_3Ni/C caused by alloying effects rather than particle size effects.

It should be noted that the rate enhancement of the structural kinetics brought by the alloying of Pt with 3d transition metals was sensitive to the voltage change of 1.0 V → 0.4 V (Pt reduction) and less sensitive to the step of 0.4 V → 1.0 V (Pt oxidation) in N_2. These trends were observed in both Pt_3Co/C and Pt_3Ni/C under identical conditions. Figure 7C revealed that the rate enhancement of the structural kinetics of the Pt catalysts has a positive correlation with the cell performance. The desorption of oxygen atoms from the surface of a Pt catalyst, that is the reduction of Pt electron state, and Pt−O bond breaking at the catalyst surface are known to be key steps in ORR.[13−23] The present results of the in situ time-resolved XAFS analysis indicated a positive contribution of Pt alloying to the rate enhancement in Pt structural kinetics with the improvement of PEFC performance.

In addition to improving PEFC performance, it is necessary to improve the resilience of cathode catalysts to oxidative dissolution of the Pt species under voltage cycling conditions. It has been suggested that oxidative dissolution of Pt cathode catalysts is caused by the delay in Pt reduction during the voltage cycling process.[8−10,57] The present study demonstrated that the alloying of Pt with 3d transition metals can result in a significant rate enhancement of the Pt reduction process,

dx.doi.org/10.1021/jp504738p | J. Phys. Chem. C 2014, 118, 15874−15883

enabling a reversible redox process of the cathode catalysts for extended durability of PEFC.

CONCLUSIONS

We acquired a series of in situ time-resolved QXAFS spectra of Pt/C, Pt_3Co/C, and Pt_3Ni/C cathode catalysts (practical catalyst loading: 0.5 mg_{metal} cm^{-2}) in MEAs in PEFCs at 100 ms intervals. Systematic analysis of the spectra provided the rate constants of the dynamic surface events on the Pt/C, Pt_3Co/C, and Pt_3Ni/C cathode catalysts in the voltage cycling process between 0.4 and 1.0 V. The Pt-based bimetallic catalysts had Pt-rich surfaces and Pt−Co/Ni bimetallic cores, and the redox reactions during the voltage cycling process took place on the Pt-rich catalyst surfaces for all three catalysts. We found notable enhancements in the rate constants of the structural kinetics, in particular, for the reductive processes of the Pt cathode catalysts, and the extent of the enhancement was related to the level of d-band centers of the Pt catalysts. In situ time-resolved XAFS analysis is a promising technique that can aid the further development of bimetallic electrocatalysts from the viewpoints of improvement of PEFC performance and durability.

ASSOCIATED CONTENT

Supporting Information

Experimental procedures, TEM, XANES, EXAFS curve fitting results, series of time-resolved XANES spectra and EXAFS Fourier transforms, profiles in air, refs 1 and 47. This material is available free of charge via the Internet at http://pubs.acs.org.

AUTHOR INFORMATION

Corresponding Author

*E-mail mtada@chem.nagoya-u.ac.jp; Fax +81-52-788-6200 (M.T.).

Notes

The authors declare no competing financial interest.

ACKNOWLEDGMENTS

This work was supported by the New Energy and Industrial Technology Development Organization of the Ministry of Economy, Trade and Industry, Japan. XAFS measurements were performed at SPring-8 (Nos. 2011B1018, 2012B1008, 2013A7820, and 2013B7820). We thank JEOL for the STEM-EDS analysis and Dr. Tadashi Ueda (Institute for Molecular Science) for TEM measurements.

REFERENCES

(1) Borup, R.; Meyers, J.; Pivovar, B.; Kim, Y. S.; Mukundan, R.; Garland, N.; Myers, D.; Wilson, M.; Garzon, F.; Wood, D.; et al. Scientific Aspects of Polymer Electrolyte Fuel Cell Durability and Degradation. *Chem. Rev.* **2007**, *107*, 3904−3951.

(2) de Bruijn, F. A.; Dam, V. A. T.; Janssen, G. J. M. Review: Durability and Degradation of PEM Fuel Cell Components. *Fuel Cells* **2008**, *8*, 3−22.

(3) Markovic, N. M.; Schmidt, T. J.; Stamenkovic, V.; Ross, P. N. Oxygen Reduction Reaction on Pt and Pt Bimetallic Surfaces: A Selective Review. *Fuel Cells* **2001**, *1*, 105−116.

(4) Paulus, U. A.; Wokaun, A.; Scherer, G. G.; Schmidt, T. J.; Stamenkovic, V.; Radmilovic, V.; Markovic, N. M.; Ross, P. N. Oxygen Reduction on Carbon-Supported Pt-Ni and Pt-Co Alloy Catalysts. *J. Phys. Chem. B* **2002**, *106*, 4181−4191.

(5) Mukerjee, S.; Srinivasan, S. Enhanced Electrocatalysis of Oxygen Reduction on Platinum Alloys in Proton Exchange Membrane Fuel Cells. *J. Electroanal. Chem.* **1993**, *357*, 201−224.

(6) Mani, P.; Srivastava, R.; Stasser, P. Dealloyed Pt-Cu Core-Shell Nanoparticle Electrocatalysts for Use in PEM Fuel Cell Cathodes. *J. Phys. Chem. C* **2008**, *112*, 2770−2778.

(7) Koh, S.; Toney, M. F.; Strasser, P. Activity-Stability Relationships of Ordered and Dissociated Alloy Phases of Pt_3Co Electrocatalysts for the Oxygen Reduction Reaction (ORR). *Electrochim. Acta* **2007**, *52*, 2765−2774.

(8) Yu, P.; Pemberton, M.; Plasse, P. PtCo/C Cathode Catalyst for Improved Durability in PEMFCs. *J. Power Sources* **2005**, *144*, 11−20.

(9) Colón-Mercado, H. R.; Popov, B. N. Stability of Platinum Based Alloy Cathode Catalysts in PEM Fuel Cells. *J. Power Sources* **2006**, *155*, 253−263.

(10) Matsutani, K.; Hayakawa, K.; Tada, T. Effect of Particle Size of Platinum and Platinum-Cobalt Catalysts on Stability Against Load Cycling. *Platinum Met. Rev.* **2010**, *54*, 223−232.

(11) Chen, S.; Sheng, W.; Yabuchi, N.; Ferreira, P. J.; Allard, L. F.; Shao-Horn, Y. Origin of Oxygen Reduction Activity on "Pt_3Co" Nanoparticles: Atomically Resolved Chemical Compositions and Structures. *J. Phys. Chem. C* **2009**, *113*, 1109−1125.

(12) Chen, S.; Gasteiger, H. A.; Hayakawa, K.; Tada, T.; Shao-Horn, Y. Platinum-Alloy Cathode Catalyst Degradation in Proton Exchange Membrane Fuel Cells: Nanometer-Scale Compositional and Morphological Changes. *J. Electrochem. Soc.* **2010**, *157*, A82−A97.

(13) Stamenkovic, V. R.; Mun, B. S.; Mayhofer, K. J. J.; Ross, P. N.; Markovic, N. M. Effect of Surface Composition on Electronic Structure, Stability, and Electrocatalytic Properties of Pt-Transition Metal Alloys: Pt-Skin versus Pt-Skelton Surfaces. *J. Am. Chem. Soc.* **2006**, *128*, 8813−8819.

(14) Stamenkovic, V. R.; Fowler, B.; Mun, B. S.; Wang, G.; Ross, P. N.; Lucas, C. A.; Marcovic, N. M. Improved Oxygen Reduction Activity on $Pt_3Ni(111)$ via Increased Surface Site Availability. *Science* **2007**, *315*, 493−497.

(15) Stamenkovic, V. R.; Mun, B. S.; Arenz, M.; Mayrhofer, K. J. J.; Lucas, C. A.; Wang, G.; Ross, P. N.; Markovic, N. M. Trends in Electrocatalysis on Extended and Nanoscale Pt-Bimetallic Alloy Surfaces. *Nat. Mater.* **2007**, *6*, 241−247.

(16) Gauthier, Y. Pt-Metal Alloy Surfaces: Systematic Trends. *Surf. Rev. Lett.* **1996**, *3*, 1663−1689.

(17) Mun, B. S.; Watanabe, M.; Rossi, M.; Stamenkovic, V.; Markovic, N. M.; Ross, P. N. A Study of Electronic Structures of Pt_3M (M = Ti, V, Cr, Fe, Co, Ni) Polycrystalline Alloys with Valence-Band Photoemission Spectroscopy. *J. Chem. Phys.* **2005**, *123*, 204717.

(18) Kitchin, J. R.; Nørskov, J. K.; Barteau, M. A.; Chen, J. G. Modification of the Surface Electronic and Chemical Properties of Pt(111) by Subsurface 3*d* Transition Metals. *J. Chem. Phys.* **2004**, *120*, 10240−10246.

(19) Xu, Y.; Ruban, A. V.; Mavrikakis, M. Adsorption and Dissociation of O_2 on Pt-Co and Pt-Fe Alloys. *J. Am. Chem. Soc.* **2004**, *126*, 4717−4725.

(20) Stamenkovic, V.; Mun, B. S.; Mayrhofer, K. J. J.; Ross, P. N.; Markovic, N. M.; Rossmeisl, J.; Greeley, J.; Nørskov, J. K. Changing the Activity of Electrocatalysts for Oxygen Reduction by Tuning the Surface Electronic Structure. *Angew. Chem., Int. Ed.* **2006**, *45*, 2897−2901.

(21) Callejas-Tovar, R.; Balbuena, P. B. Oxygen Adsorption and Surface Segregation in (211) Surfaces of Pt(Shell)/M(Core) and Pt_3M (M = Co, Ir) Alloys. *Surf. Sci.* **2008**, *602*, 3531−3539.

(22) Hirunsit, P.; Balbuena, P. B. Effects of Water and Electric Field on Atomic Oxygen Adsorption on Pt-Co Alloys. *Surf. Sci.* **2009**, *603*, 3239−3248.

(23) Matanovic, I.; Garzon, F. H.; Henson, N. J. Theoretical Study of Electrochemical Processes on Pt-Ni Alloys. *J. Phys. Chem. C* **2011**, *115*, 10640−10650.

(24) Xin, H. L.; Mundy, J. A.; Liu, Z.; Cabezas, R.; Hoven, R.; Kourkoutis, L. F.; Zhang, J.; Subramanian, N. P.; Makharia, R.; Wagner, F. T.; Muller, D. A. Atomic-Resolution Spectroscopic Imaging of Ensembles of Electrocatalyst Particle across the Life of a Fuel Cell. *Nano Lett.* **2012**, *12*, 490−497.

(25) Carlton, C. E.; Chen, S.; Ferreira, P. J.; Allard, L. F.; Shao-Horn, Y. Sub-Nanometer-Resolution Elemental Mapping of "Pt_3Co" Nanoparticle Catalyst Degradation in Proton-Exchange Membrane Fuel Cells. *J. Phys. Chem. Lett.* **2012**, *3*, 161−166.
(26) Durst, J.; Lopez-Haro, M.; Dubau, L.; Chatenet, M.; Soldo-Olivier, Y.; Guétaz, L.; Bayle-Guillemaud, P.; Maillard, F. Reversibility of Pt-Skin and Pt-Skeleton Nanostructures in Acidic Media. *J. Phys. Chem. Lett.* **2014**, *5*, 434−439.
(27) Yu, Y.; Xin, H. L.; Hovden, R.; Wang, D.; Rus, E. D.; Mundy, J. A.; Muller, D. A.; Abruña, H. Three-Dimensional Tracking and Visualization of Hundreds of Pt-Co Fuel Cell Nanocatalysts during Electrochemical Aging. *Nano Lett.* **2012**, *12*, 4417−4423.
(28) Heggen, M.; Oezaslan, M.; Houben, L.; Strasser, P. Formation and Analysis of Core-Shell Fine Structures in Pt Bimetallic Nanoparticle Fuel Cell Electrocatalysts. *J. Phys. Chem. C* **2012**, *116*, 19073−19083.
(29) Menning, C. A.; Hwu, H. H.; Chen, J. G. Experimental and Theoretical Investigation of the Stability of Pt-3*d*-Pt(111) Bimetallic Surfaces under Oxygen Environment. *J. Phys. Chem. B* **2006**, *110*, 15471−15477.
(30) Doung, H. T.; Rigsby, M. A.; Zhou, W.-P.; Wieckowski, A. Oxygen Reduction Catalysis of the Pt_3Co Alloy in Alkaline and Acidic Media Studied by X-ray Photoelectron Spectroscopy and Electrochemical Methods. *J. Phys. Chem. C* **2007**, *111*, 13460−13465.
(31) Wakisaka, M.; Suzuki, H.; Mitsui, S.; Uchida, H.; Watanabe, M. Increased Oxygen Coverage at Pt-Fe Alloy Cathode for the Enhanced Oxygen Reduction Reaction Studied by EC-XPS. *J. Phys. Chem. C* **2008**, *112*, 2750−2755.
(32) Yu, X.; S. Ye, S. Recent Advances in Activity and Durability Enhancement of Pt/C Catalytic Cathode in PEMFC Part II: Degradation Mechanism and Durability Enhancement of Carbon Supported Platinum Catalyst. *J. Power Sources* **2007**, *172*, 145−154.
(33) Newton, M. A. Dynamic Adsorbate/Reaction Included Structural Change of Supported Metal Nanoparticles: Heterogeneous Catalysts and Beyond. *Chem. Soc. Rev.* **2008**, *37*, 2644−2657.
(34) Frenkel, A. I. Applications of Extended X-ray Absorption Fine-Structure Spectroscopy to Studies of Bimetallic Nanoparticle Catalysts. *Chem. Soc. Rev.* **2012**, *41*, 8163−8178.
(35) Bordiga, S.; Groppo, E.; Agostini, G.; von Bokhove, J. A.; Labberti, C. Reactivity of Surface Species in Heterogeneous Catalysts Probed by in Situ X-ray Absorption Techniques. *Chem. Rev.* **2013**, *113*, 1736−1850.
(36) Mukerjee, S.; Srinivasan, S.; Soriaga, M. P.; McBreen, J. Role of Structural and Electronic Properties of Pt and Pt Alloys on Electrocatalysis of Oxygen Reduction. *J. Electrochem. Soc.* **1995**, *142*, 1409−1422.
(37) Teliska, M.; Murthi, V. S.; Mukerjee, S.; Ramaker, D. E. Correlation of Water Activation, Surface Properties, and Oxygen Reduction Reactivity of Supported Pt-M/C Bimetallic Electrocatalysts Using XAS. *J. Electrochem. Soc.* **2005**, *152*, A2159−A2169.
(38) Antolini, E.; Salgado, J. R. C.; Giz, M. J.; Gonzalez, E. R. Effects of Geometric and Electronic Factors on ORR Activity of Carbon Supported Pt-Co Electrocatalysts in PEM Fuel Cells. *Int. J. Hydrogen Energy* **2005**, *30*, 1213−1220.
(39) Witkowska, A.; Dsoke, S.; Principi, E.; Marassi, R.; Di Cicco, A.; Albertini, V. R. Pt-Co Cathode Electrocatalyst Behaviour Viewed by In Situ XAFS Fuel Cell Measurements. *J. Power Sources* **2008**, *178*, 603−609.
(40) Lai, F.-J.; Sarma, L. S.; Chou, H.-L.; Liu, D.-G.; Hsieh, C.-A.; Lee, J.-F.; Hwang, B. J. Architecture of Bimetallic Pt_xCo_{1-x} Electrocatalysts for Oxygen Reduction Reaction As Investigated by X-ray Absorption Spectroscopy. *J. Phys. Chem. C* **2009**, *113*, 12674−12681.
(41) Lai, F.-J.; Su, W.-N.; Sarma, L. S.; Liu, D.-G.; Hsieh, C.-A.; Lee, J.-F.; Hwang, B.-J. Chemical Dealloying Mechanism of Bimetallic Pt-Co Nanoparticles and Enhancement of Catalytic Activity toward Oxygen Reduction. *Chem.—Eur. J.* **2010**, *16*, 4602−4611.
(42) Greco, G.; Witkowska, A.; Minicucci, M.; Olivi, L.; Principi, E.; Dsoke, S.; Moretti, A.; Marassi, R.; Di Cicco, A. Local Ordering Changes in Pt-Co Nanocatalysts Induced by Fuel Cell Working Conditions. *J. Phys. Chem. C* **2012**, *116*, 12791−12802.
(43) Ishiguro, N.; Saida, T.; Uruga, T.; Nagamatsu, S.; Sekizawa, O.; Nitta, K.; Yamamoto, T.; Ohkoshi, S.; Iwasawa, Y.; Yokoyama, T.; Tada, M. Operando Time-Resolved X-ray Absorption Fine Structure Study for Surface Events on a Pt_3Co/C Cathode Catalyst in a Polymer Electrolyte Fuel Cell during Voltage-Operating Processes. *ACS Catal.* **2012**, *2*, 1319−1330.
(44) Ishiguro, N.; Saida, T.; Uruga, T.; Sekizawa, O.; Nagasawa, K.; Nitta, K.; Yamamoto, T.; Ohkoshi, S.; Yokoyama, T.; Tada, M. Structural Kinetics of a Pt/C Cathode Catalyst with Practical Catalyst Loading in an MEA for PEFC Operating Conditions Studied by In Situ Time-Resolved XAFS. *Phys. Chem. Chem. Phys.* **2013**, *15*, 18827−18834.
(45) Kityakarn, S.; Saida, T.; Sode, A.; Ishiguro, N.; Sekizawa, O.; Uruga, T.; Nagasawa, K.; Yamamoto, T.; Yokoyama, T.; Tada, M. In Situ Time-Resolved XAFS of Transitional States of Pt/C Cathode Electrocatalyst in an MEA during PEFC Loading with Transient Voltages. *Top. Catal.* **2014**, *57*, 903−910.
(46) Hashimasa, Y.; Numata, T.; Moriya, K.; Watanabe, S. Development of JARI Standard Single Cell for Testing Cell Materials (1). *JARI Res. J.* **2002**, *24*, 455−458.
(47) Sekizawa, O.; Uruga, T.; Tada, M.; Nitta, K.; Kato, K.; Tanida, H.; Takeshita, K.; Takahashi, S.; Sano, M.; Aoyagi, H.; et al. New XAFS Beamline for Structural and Electronic Dynamics of Nanoparticle Catalysts in Fuel Cells under Operating Conditions. *J. Phys. Conf. Ser.* **2013**, *430*, 012020.
(48) Newville, M.; Ravel, B.; Haskel, D.; Rehr, J. J.; Stern, E. A.; Yacoby, Y. Analysis of Multiple-Scattering XAFS Data Using Theoretical Standards. *Phys. B* **1995**, *208−209*, 154−156.
(49) Moreno, M. S.; Jorissen, K.; Rehr, J. J. Practical Aspects of Electron Energy-Loss Spectroscopy (EELS) Calculations Using FEFF8. *Micron* **2007**, *38*, 1−11.
(50) Ankudinov, A. L.; Nesvizhskii, A. I.; Rehr, J. J. Dynamic Screening Effects in X-ray Absorption Spectra. *Phys. Rev. B* **2003**, *67*, 115120.
(51) Davey, W. P. Precision Measurements of the Lattice Constants of Twelve Common Metals. *Phys. Rev.* **1925**, *25*, 753−761.
(52) Muller, O.; Roy, R. Formation and Stability of the Platinum and Rhodium Oxides at High Oxygen Pressures and the Structures of Pt_3O_4, β-PtO_2 and RhO_2. *J. Less-Common Met.* **1968**, *16*, 129−146.
(53) Buschow, K. H. J.; van Engen, P. G.; Jongebreur, R. Magnrto-Optical Properties of Metallic Ferromagnetic Materials. *J. Magn. Magn. Mater.* **1983**, *38*, 1−22.
(54) Leroux, C.; Cadeville, M. C.; Pierron-Bohnes, V.; Inden, G.; Hinz, F. Comparative Investigation of Structural and Transport Properties of $L1_0$ NiPt and CoPt Phases; The Role of Magnetism. *J. Phys. F: Met. Phys.* **1988**, *18*, 2033−2051.
(55) Nesselberger, M.; Ashton, S.; Meier, J. C.; Katsounaros, I.; Mayrhofer, K. J. J.; Arenz, M. The Particle Size Effect on the Oxygen Reduction Reaction Activity of Pt Catalysts: Influence of Electrolyte and Relation to Single Crystal Models. *J. Am. Chem. Soc.* **2011**, *133*, 17428−17433.
(56) Perez-Alonso, F. J.; McCarthy, D. N.; Nierhoff, A.; Hernandez-Fernandez, P.; Strebel, C.; Steohens, I. E. L.; Nielsen, J. H.; Chorkenfdorff, I. The Effect of Size on the Oxygen Electroreduction Activity of Mass-selected Platinum Nanoparticles. *Angew. Chem., Int. Ed.* **2012**, *51*, 4641−4643.
(57) Imai, H.; Matsumoto, M.; Miyazaki, T.; Kato, K.; Tanida, H.; Uruga, T. Growth Limits on Platinum Oxides Formed on Pt-Skin Layers on Pt-Co Bimetallic Nanoparticles. *Chem. Commun.* **2011**, *47*, 3538−3540.